The Conformational and Dynamic Basis for Ligand Binding Reactivity in Hemoglobin Ypsilanti (β99 Asp→Tyr): Origin of the Quaternary Enhancement Effect†

J. Huang, L. J. Juszczak, E. S. Peterson, C. F. Shannon, M. Yang, S. Huang, G. V. A. Vidugiris, and J. M. Friedman*

Department of Physiology and Biophysics, Albert Einstein College of Medicine, Bronx, New York 10461

Received November 16, 1998; Revised Manuscript Received February 4, 1999

ABSTRACT: Hemoglobin Ypsilanti (HbY) is a stable tetrameric hemoglobin that binds oxygen with little or no cooperativity and with high affinity [Doyle, M. L., et al. (1992) *Proteins: Struct., Funct., Genet. 14*, 351−362]. It displays an especially large quaternary enhancement effect. An X-ray crystallographic study [Smith, F. R., et al. (1991) *Proteins: Struct., Funct., Genet. 10*, 81−91] of the carboxy derivative of this hemoglobin (COHbY) revealed a new quaternary structure that partially resembles the recently described R_2 structure [Silva, M. M., et al. (1992) *J. Biol. Chem. 267*, 17248−17256]. Very little is known about either the solution phase conformations of the liganded and deoxy forms of HbY or the molecular basis for the large quaternary enhancement effect (Doyle et al., 1992). In this study, near-IR absorption, Soret-enhanced Raman, and UV (229 nm) resonance Raman spectroscopies are used to probe the liganded and deoxy derivatives of HbY in solution. Nanosecond time-resolved near-IR absorption measurements are used to expose the relaxation properties of the photoproduct of COHbY. Time-resolved (Soret band) absorption is used to generate the geminate and solvent phase ligand rebinding curves for photodissociated COHbY. The spectroscopic results indicate that COHbY has an R-like conformation with respect to both the proximal heme pocket and the hinge region of the $\alpha_1\beta_2$ interface. The deoxy derivative of HbY has spectroscopic features that are very similar to those observed for species assigned to the deoxy R or half-liganded R conformations of human adult hemoglobin (HbA). The 10 ns to 100 μs relaxation properties of the photoproduct of COHbY are distinctly different from those of HbA in that for HbY, little if any tertiary or quaternary relaxation is observed. The near-absence of relaxation in the HbY photoproduct explains the differences in the geminate and solvent phase CO recombination between HbA and HbY. The impact of the conformational and relaxation properties of HbY on the geminate rebinding process forms the basis of a model that accounts for the large quaternary enhancement effect reported for HbY (Doyle et al., 1992). In addition, the spectroscopic data and the X-ray crystallographic results explain the slow relaxation for HbY and the near-absence of cooperative ligand binding for this protein based on the behavior of the penultimate tyrosines.

Hemoglobin plays an important role in the understanding of the allosteric regulation in proteins. Early crystallographic and thermodynamic studies revealed two stable quaternary structures (often referred to as states) (*4*). The T and R quaternary structures are observed for crystals of the equilibrium deoxy and liganded forms of HbA, respectively. Many studies indicate that the ligand binding and allosteric effector dependent shift between the low-affinity T and the high-affinity R structures is responsible for the overall features of cooperative ligand binding in hemoglobin. It appeared that hemoglobin was a near-perfect model system exemplifying two-state MWC allostery. With increasing biophysical and biochemical sophistication came more rigorous tests and questions regarding the molecular basis for cooperativity. Such studies have yielded indications of additional states that might contribute to and hence complicate the allosteric mechanism (*5*).

Recently it was shown (*2*) that the CO derivative of Hb Ypsilanti (β99 Asp→Tyr) crystallizes in a new third quaternary structure, called the Y structure, that is distinctly unique from the classic T and R structures. Subsequently, other similar structures, such as the R2 structure, were found for liganded HbA crystallized under varying conditions (*3, 6, 7*). Both Y and R2 are clearly part of a family of R-like structures that also includes the initially described R state (A. Arnone, personal communication). The nature of the deoxy derivative of HbY is not apparent from these studies. It has been proposed that the Y or R2 structure may be associated with the last ligand binding step in HbA (*8*) and that the R structure is actually along the pathway between T and Y (or R2) (*7*−*10*).

Functionally, Hb Ypsilanti is a noncooperative, very high affinity Hb that exhibits two very unusual features (*1*). The first is that unlike most Hbs, the tetramer of the liganded

† This work was supported in part through NIH Grants P01HL51084 and R01Hl58247 and through the W. M. Keck Foundation.

* To whom correspondence should be addressed. Phone: 718 430 3591. FAX: 718 430 8819. Email: jfriedma@aecom.yu.edu.

10.1021/bi982724h CCC: $18.00
Published on Web 03/19/1999

form of Hb Ypsilanti is more stable than the deoxy tetramer. The second unusual feature is that Hb Ypsilanti exhibits a very large quaternary enhancement effect; i.e., the ligand binding affinity for each of the four ligation steps is markedly higher than for the free $\alpha\beta$ dimer. In HbA, only the last ligand binding step occurs with the enhanced (over the dimer) affinity. This quaternary enhancement effect indicates that the quaternary/tertiary structure of the tetramer of Hb Ypsilanti significantly enhances ligand affinity over that of the free dimer. As with many other β99 Hb mutants, HbY does not exhibit the reduced affinity associated with the T state tetramer (*1*). Thus, for HbY, the quaternary constraint associated with the binding of the first ligand is abolished and all four ligands bind to the tetramer with greater affinity than for the isolated $\alpha_1\beta_1$ dimers. The origin of these effects is unclear based on the existing crystal structure.

In the present study, several optical spectroscopic tools are used to probe the solution phase properties of HbY. Visible resonance Raman spectroscopy is used to probe the heme and heme environment of both equilibrium and nonequilibrium forms of the deoxy protein. In particular, this study utilizes the nonequilibrium deoxy species generated within 10 ns of photodissociating the CO-saturated derivatives of HbA and HbY as means of probing the influence of the initial unrelaxed liganded protein tertiary and quaternary structure upon a ferrous five-coordinate heme. Thus, a direct comparison can be made of the influence of the equilibrium deoxy or liganded protein conformations upon the same molecular chromophore, i.e., a ferrous five-coordinate heme. Ultraviolet resonance Raman spectroscopy is used to probe the $\alpha_1\beta_2$ interface in both the deoxy and CO derivatives. Functional studies of this protein take the form of transient absorption measurements after photodissociation which are used to generate profiles of the geminate and solvent-derived ligand rebinding processes.

Relaxation of the heme environment after photodissociation is followed from 10 ns to 50 μs using a near-IR charge-transfer absorption band as a local probe. This weak but spectrally well-isolated iron−porphyrin charge-transfer absorption band (*11*) is associated with five-coordinate high-spin ferrous heme and has been shown to be sensitive to both subunit and protein conformations (*12*−*14*). Kinetic hole burning experiments show that this band is inhomogeneously broadened due to a distribution of conformational substates having different heme environments (*13*−*17*). The wavelength of the composite band is sensitive to both quaternary and tertiary structure (*13, 18*). Time-resolved band III absorption studies can be used to follow the influence of both tertiary and quaternary relaxations upon the iron (*18*−*20*). For those hemeproteins having a distal histidine, the wavelength of band III correlates with the frequency of ν(Fe−His), the iron−proximal histidine stretching mode (*13, 18, 21, 22*). Large reductions in the polarity of the distal pocket (due to mutagenesis) result in band III shifting to longer wavelengths (e.g., 768 nm for the H64L mutant of myoglobin) without concomitant change in ν(Fe−His) (*21, 22*). Thus, it appears that for Hb, where there are no large changes in polarity of the distal pocket and where shifts in band III correlate with ν(Fe−His), band III is reflective of variations in the proximal heme pocket environment. For hemoglobin, a shift of band III to longer wavelength is interpreted as a decrease in proximal strain, which implies a reduction in the potential energy barrier controlling iron−ligand bond formation.

METHODS AND MATERIALS

HbA. Human adult hemoglobin (HbA) was obtained as a gift from Drs. S. Acharya and R. Hirsch (Division of Hematology, The Albert Einstein College of Medicine). The HbA was isolated from whole blood, highly purified, and tested for purity using standard procedures. The deoxy derivative was prepared by first flushing an oxy sample with nitrogen or argon gas and then adding a 3-fold molar (heme) excess of sodium dithionite (freshly prepared anaerobic solution). The carboxy derivative was prepared in a similar fashion with the added and final step of saturating the resulting deoxy sample with CO.

HbY. Two samples of hemoglobin Ypsilanti were obtained as generous gifts from the laboratory of Dr. Gary Ackers (Department of Biochemistry, Washington University). One sample was highly purified and contained no other detectable hemoglobins. The other sample, which was not as completely purified, contained an additional hemoglobin that represented between 5 and 10% of the total hemoglobin population. The lack of additional sample material necessitated the use of the impure sample since the required additional purification step needed to remove the impurity would result in the loss of some HbY. For the spectroscopic measurements, an impurity at the level of 10% or lower is not expected to be a complicating factor. Kinetic measurements on both samples yielded sufficiently similar results so as not to pose ambiguities in the analysis.

The time-resolved near-IR absorption studies were conducted on the fully purified COHbY samples (approximately 1 mM in heme) in a pH 7.4 buffer containing 0.1 M Tris, 0.1 M NaCl, and 1 mM Na_2EDTA. Visible resonance Raman measurements were made on solutions of HbY in the above Tris buffer as well as in a 50 mM pH 7.4 Hepes buffer. UV resonance Raman measurements were conducted on samples in 50 mM Hepes, pH 7.4, with the addition of 0.3 M sodium perchlorate as an internal intensity standard. Samples in both buffers were also used in the ligand rebinding studies.

Near-IR Absorption: Band III at ~760 nm. Nanosecond time-resolved near-IR absorption spectra of the photoproducts of both COHbA and COHbY were obtained using a double-laser apparatus that is described in earlier work (*19, 20*). The apparatus utilizes a flowing stream of a mix of laser dyes which produce an approximately 10 ns continuum of wavelengths in the near-IR region of the spectrum when pumped with the 7 ns second harmonic output of a Nd:YAG laser. This continuum is used as a probe beam to interrogate the sample after photodissociation. A second Nd:YAG laser is used to produce the 7 ns green pulses used to photodissociate the interrogated volume of sample. The two lasers are triggered via the same delay generator to allow for the systematic tuning of the time delay between the photolysis and probe pulses. Spectra at time delays extending from 10 ns out to a few hundred microseconds were generated in a nonsequential manner in that short and long delays were intermixed. Spectra at all time points were generated several times on the same sample at different times during the course of an experiment and compared to ensure reproducibility. In virtually all cases the spectra at a given time delay were

identical regardless of whether they were generated early or late in the sequence of data acquisition.

Visible Resonance Raman Spectra. The resonance Raman spectra of the equilibrium deoxy derivatives and the photoproducts of the CO-bound derivatives of HbA and HbY were obtained using a Raman apparatus described in detail in an earlier paper (*23*). Briefly, Soret band enhanced time-resolved Raman spectra were obtained using an 8 ns, 150 μJ 435.8 nm pulse to both photodissociate the ligand (in the case of the CO derivatives) and Raman scatter off the sample. The laser used was a frequency-doubled Nd:YAG laser (Continuum NY81C-20, Santa Clara, CA) that was frequency shifted via stimulated Raman scattering in a hydrogen cell. The detector was an intensified diode array run in the cw mode (Princeton Instruments, P/N IRY-1024S/B, Trenton, NJ). The spectral bandwidth of the monochromator was approximately 2.5 cm^{-1}, and the resolution of the detector array was approximately 0.9 cm^{-1} per pixel. Raman spectra were calibrated using solvent spectra with previously determined peak assignments. A least-squares fit was used to map pixel number into relative wavenumbers (Raman shift), and the resulting Raman shift values are estimated to be accurate to within ± 0.25 cm^{-1}. The Raman spectra were base lined using a polynomial fitting routine in LabCalc (Galactic Industries, Salem NH), normalized in intensity using the ν_7 mode band at $\sim$672 cm^{-1}, and are presented without smoothing. In the present study, the sample is contained in either a spinning NMR tube or a special disk-shaped holder described previously (*23*). The focus in this study is on the low-frequency portion of the Raman spectrum that is especially sensitive to both quaternary and tertiary conformation changes.

UV Resonance Raman Spectra. The cw UV resonance Raman spectra of the deoxy and CO-bound derivatives of HbA and HbY were generated using the 229 nm output of a frequency-doubled argon ion laser (1.8 mW at the sample). The Raman scattered light was collected, dispersed, and detected using a previously described (*24*, *25*) UV Raman apparatus derived from a single spectrograph with a CCD detector. As in previous UV Raman studies, the 934 cm^{-1} perchlorate band is used as an internal Raman intensity standard.

Ligand Rebinding. The nanosecond geminate recombination and the slower solvent-derived bimolecular recombination of photodissociated COHbA and COHbY were obtained using a modified version of a previously described flash photolysis apparatus (*26*). The flash photolysis apparatus for the carbon monoxide rebinding rate experiments used the frequency-doubled output of a Nd:YAG laser (Continuum Surelite, Santa Clara, CA) at 532 nm to photolyze the carbonmonoxy hemoglobin. The photolysis pulses were approximately 8 ns in duration with a 2 Hz repetition rate and were focused to a diameter of about 2 mm on the sample with a 1000 mm focal length lens located 800 mm from the sample. Maximum photolysis within the illuminated sample volume was achieved by increasing the Nd:YAG laser pulse energy until the maximum change in optical density was obtained. This typically required an energy of about 0.33 mJ per pulse. Recombination of the CO was monitored by measuring the change in sample absorption at 441.6 nm using the cw output of a HeCd laser (Liconix, P/N 4240NB, Santa Clara, CA). The position of the illuminated volume on the sample was not changed during the flash photolysis measurements. The unfocused HeCd probe laser beam passed through the sample nearly collinear with the Nd:YAG beam and was separated from the 532 nm light using a dichroic optic and a single monochromator with a 638 line/mm grating (Varian, P/N MC-6, Sugarland, TX). The light intensity at the exit slit of the monochromator was measured with a 2.2 ns rise time photomultiplier tube (Hamamatsu, P/N R105UH, Bridgewater, NJ) whose output was amplified with a 95 MHz preamplifier (Comlinear Corp., P/N E201, Fort Collins, CO). The detector output was digitized with a 500 MHz digital oscilloscope (LeCroy, P/N 7200 with a 7242B plug-in, Chestnut Ridge, NJ), and traces for 1000 laser shots were averaged. The recombination kinetics on the nanosecond, microsecond, and millisecond time scales were measured separately using a 10 000 point trace collected with a digitizing rate of 1 ns, 100 ns, and 50 μs per point, respectively. A multipoint smoothing was applied to portions of the trace before storage on a 486 computer (Gateway 2000, P/N 4DX-33, North Sioux City, SD). The measured voltages were converted to survival probabilities (normalized changes in optical density) by subtracting the base 10 logarithm of the time-dependent voltage from the logarithm of the average voltage value measured before the photolysis pulse arrival and then normalized using the maximum change in optical density. The survival probabilities were fit to a sum of exponential functions using a nonlinear least-squares algorithm that employs a sequential quadratic programming method available in the MATLAB programming package (The Mathworks, Natick, MA).

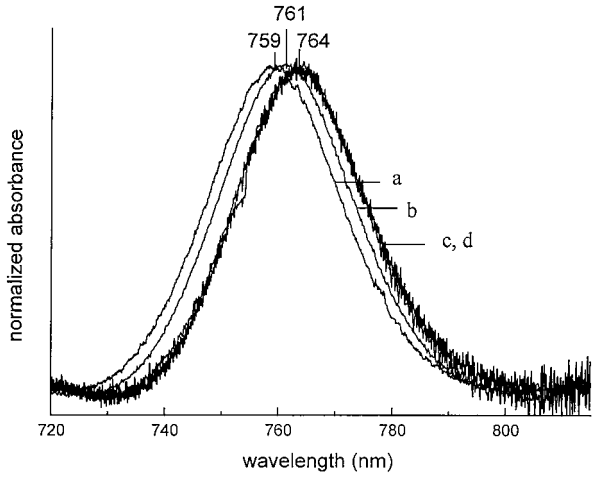

FIGURE 1: Intensity-normalized profile of band III for (a) deoxyHbA, (b) deoxyHbY, and (c and d) the photoproducts at 10 ns of COHbA and COHbY, respectively.

Sample Integrity. The oxidation state, degree of ligation, and degree of degradation were determined by measuring the absorption spectra of samples before and after each data acquisition on a Perkin-Elmer UV/VIS spectrometer. A protocol was developed that allowed for the generation of the absorption spectrum from small volumes of sample within NMR tubes.

RESULTS

Near-IR Absorption. Figure 1 shows the intensity-normalized near-IR porphyrin to iron charge-transfer absorption bands (referred to as band III) for the equilibrium deoxy and

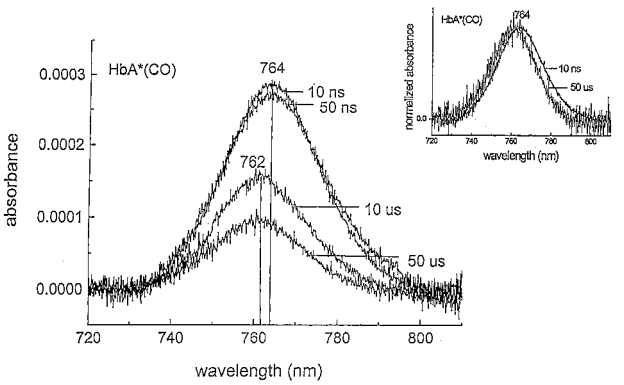

FIGURE 2: Time evolution of band III for photodissociated COHbA. The insert compares the intensity-normalized band III at 10 ns and 50 μs.

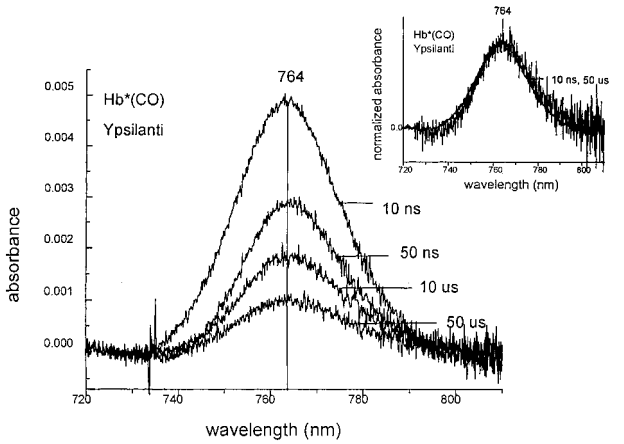

FIGURE 3: Time evolution of band III for photodissociated COHbY. The insert compares the intensity-normalized band III at 10 ns and 50 μs.

the early time (10 ns) photoproduct forms of HbA and HbY. The photoproducts are derived from the CO-bound derivatives and are referred to henceforth as HbX*(*t*), where *t* is the time after the initial photolytic event and X is the species of Hb (A or Y). The peak positions for HbA*(10 ns) and HbY*(10 ns) are both at 764 nm. In contrast, the equilibrium deoxyHbs have different peak positions with HbA at 759 nm and HbY at 761 nm.

Figure 2 shows band III for HbA*(*t*) at several time delays after photodissociation. It can be seen that with increasing time, the overall intensity decreases and the peak position shifts to shorter wavelengths. The decrease in intensity is due to ligand rebinding (the six-coordinate species does not exhibit a band in this region of the spectrum). The insert compares the intensity normalized bands for the transients at 10 ns and at 50 μs. It can be seen that the peak position shifts to bluer wavelengths with increasing delays. Figure 3 shows a similar sequence for HbY*(*t*). As with HbA*, band III for HbY* loses intensity with increasing delays. The insert in Figure 3 compares the intensity-normalized band III at 10 ns and 50 μs. In contrast to HbA*, band III for HbY* undergoes minimal peak shifting on the nanosecond to tens of microseconds time scale after photodissociation. A comparison of band III for HbA* and HbY* as a function of time reveals that at 10 ns the photoproduct spectra of the two proteins can be superimposed; however, by 100 ns band III for HbA* but not HbY* has begun to relax. A plot (not shown) of band III peak intensity versus time delay for HbA*

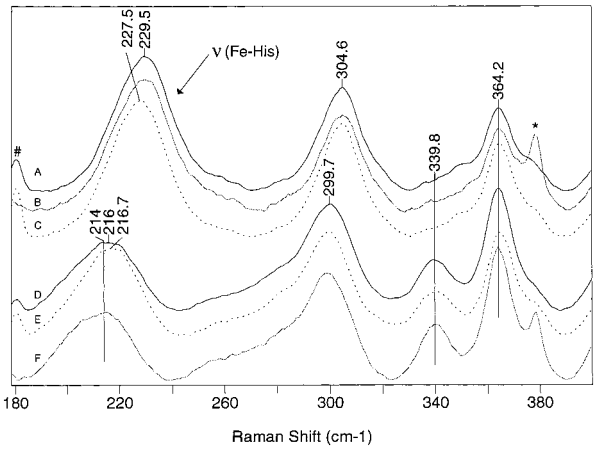

FIGURE 4: The 435.8 nm excited resonance Raman spectra of: (A) HbY*(10 ns) in 0.05 M Hepes, pH 7.4; (B) HbA*(10 ns) in 0.05 M Hepes, pH 7.4; (C) HbY*(10 ns) in 0.05 M Hepes, pH 7.4, plus 0.3 M perchlorate; (D) deoxyHbY in 0.05 M Hepes, pH 7.4, plus 0.3 M perchlorate; (E) deoxyHbY in 0.05 M Hepes, pH 7.4; and (F) deoxyHbA in 0.05 M Hepes, pH 7.4. The star and the pound symbols label reference Raman lines from a sapphire window and a hydrogen-filled Raman shifter, respectively. The samples were maintained at 4 °C during the data acquisition.

and HbY* reveals that the decrease in intensity (i.e., the ligand rebinding) for HbY* is more extensive and more rapid. A preliminary study of the rate and extent of relaxation for band III for HbA* as a function of ionic strength indicates that the relaxation is slowed at low ionic strength.

Visible Resonance Raman Spectra. Figure 4 shows a comparison of the low-frequency region of the resonance Raman spectra of deoxyHbA, deoxyHbY, HbA*(10 ns), and HbY*(10 ns). It can be seen that the low-frequency peak (located between 214 and 229 cm^{-1}) assigned to ν(Fe−His), the iron−proximal histidine stretching mode, increases in frequency in going from deoxyHbA to deoxyHbY to HbA*(10 ns) = HbY*(10 ns). Whereas the 214 cm^{-1} frequency of ν(Fe−His) for deoxyHbA is independent of buffer and added effectors, the frequencies of ν(Fe−His) for the other species are solvent dependent. The COHbA and COHbY photoproducts at pH 7.4 exhibit a frequency of 229 cm^{-1} for low ionic strength buffers. The frequency shifts to slightly lower frequency (227 cm^{-1}) with the addition of the 0.3 M perchlorate internal standard (for UVRR) and still lower to 225−226 cm^{-1} in 0.1 M Tris plus 0.1 M NaCl or 0.1 M phosphate. The deoxyHbY sample exhibits an increase in frequency from 216 to 216.7 cm^{-1} to approximately 222 cm^{-1} in switching the buffer from low ionic strength Hepes to Hepes plus 0.3 M perchlorate to the 0.1 M Tris plus 0.1 M NaCl, respectively.

UV Resonance Raman Spectra. Figures 5, 6, 7, and 8 show comparisons of the high-frequency region of the 229 nm excited resonance Raman spectra of deoxyHbA versus COHbA, deoxyHbY versus COHbY, COHbA versus COHbY, and deoxyHbA versus deoxyHbY, respectively. At this excitation wavelength, most, if not all, of the major features in the spectra are derived from vibrational modes of tyrosine and tryptophan (*27*, *28*). In Figure 5, top, the previously reported (*29*−*33*) deoxy T minus liganded R difference spectrum for HbA is shown for reference purposes. Note that in this difference spectrum, the intensity at 1550 cm^{-1} corresponds to the low frequency shoulder of the W3 band. It can be seen from Figure 6a that the corresponding T minus

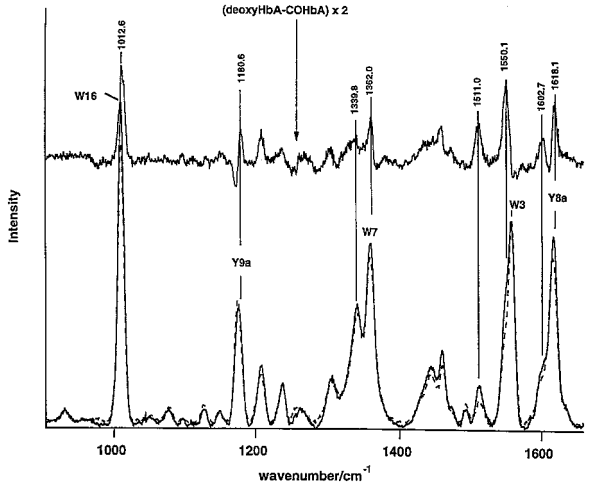

FIGURE 5: The 229 nm excited resonance Raman spectra of deoxyHbA (solid line, bottom) and COHbA (dashed line) in 0.05 M Hepes, pH 7.4, plus 0.3 M highly pure sodium perchlorate. Note that in the difference spectrum, the intensity at 1550 cm^{-1} corresponds to the low-frequency shoulder of the W3 band.

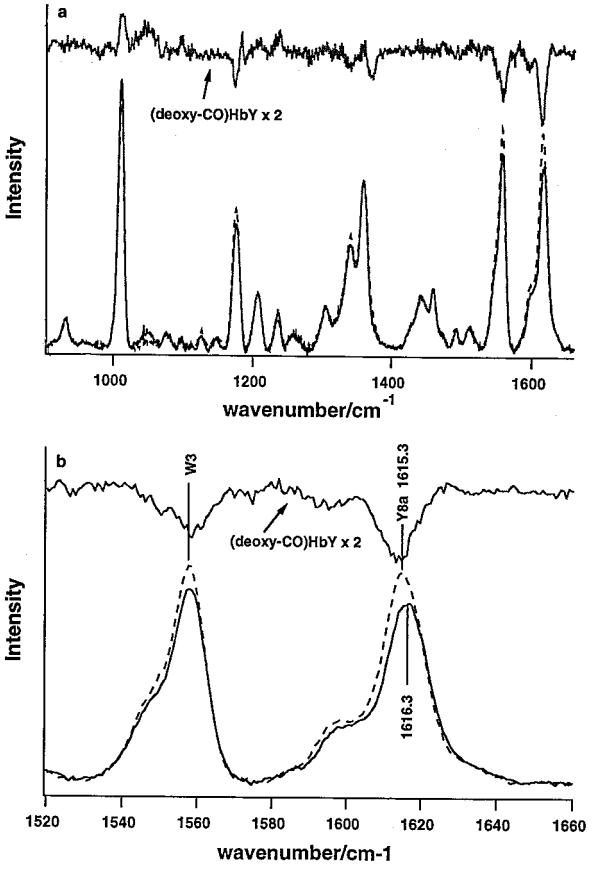

FIGURE 6: (a) The 229 nm excited resonance Raman spectra of deoxyHbY (solid line, bottom) and COHbY (dashed line) under the same conditions as in Figure 5. A blowup of the W3 and Y8a bands and the corresponding expanded difference spectrum, deoxyHbY − COHbY, are shown in (b).

R difference spectrum for HbY is quite different. Most notably, the differences are mainly due to intensity differences without significant shifting of frequencies. In Figures 6b, 7b, and 8b, the conformationally sensitve W3 and Y8a bands are shown in detail.

The deoxy versus CO difference spectra for either HbA or HbY were obtained using perchlorate as an internal

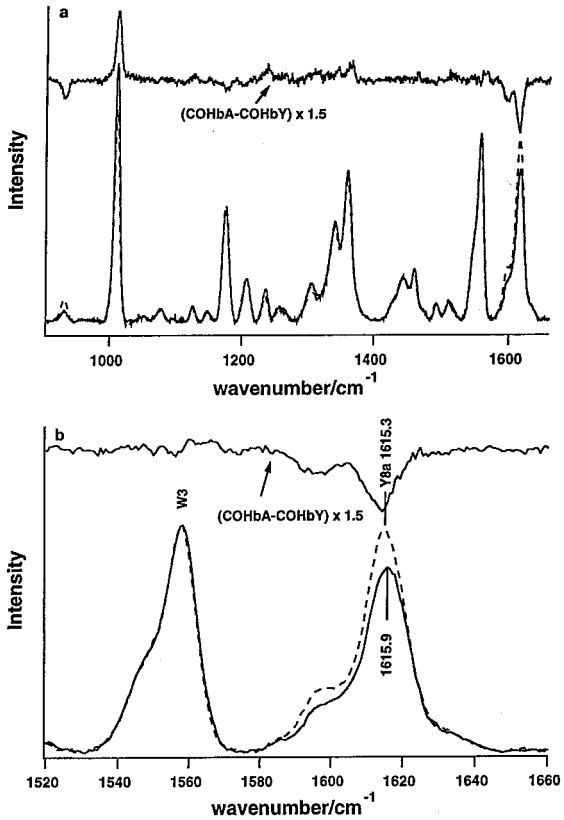

FIGURE 7: (a) Comparison of the UV resonance Raman spectra of COHbA (solid line, bottom) and COHbY (dashed line) utilizing the appropriate spectra from Figures 5 and 6. A blowup of the W3 and Y8a bands and the corresponding expanded difference spectrum, COHbA − COHbY, are shown in (b).

standard. Small variations in the concentration of perchlorate between HbA and HbY samples made it difficult to generate HbA versus HbY difference spectra by directly utilizing the perchlorate as an internal standard. The comparison between COHbA and COHbY (Figure 7) was derived by normalizing the spectra at the main peak of the W3 band. Several independent measurements indicate that W3 has the same intensity for both CO-saturated species. The comparison between the two deoxyHb spectra (Figure 8) was then achieved by scaling the reference percholorate bands to those in the W3-normalized, COHb spectra (Figure 7). The validity of this approach follows from the observation that the perchlorate band intensity remained the same for each deoxyHb−COHb comparison for a specific Hb type (Figures 5a and 6a). Similar results to those shown in Figure 7 were observed for deoxyHbY and COHbY in 0.1 M Tris, 0.1 M NaCl at the same heme concentration but lacking sufficient perchlorate to provide an adequate reference signal (data not shown).

Ligand Rebinding. Figure 9 is a log−log plot showing a comparison of the ligand rebinding as a function of time for photodissociated COHbA and COHbY after photolysis with an 8 ns pulse. On a log−log plot, k^{-1}, where k is the kinetic constant for an exponential process, can be visually determined from where the curve or extrapolation of the curve intersects the x axis. On such plots an exponential process appears as a plateau followed by a near-vertical drop in the region where $t = k^{-1}$.

The fast nonexponential phase occurring on the 100 ns time scale is geminate recombination (*34*−*37*), whereas the

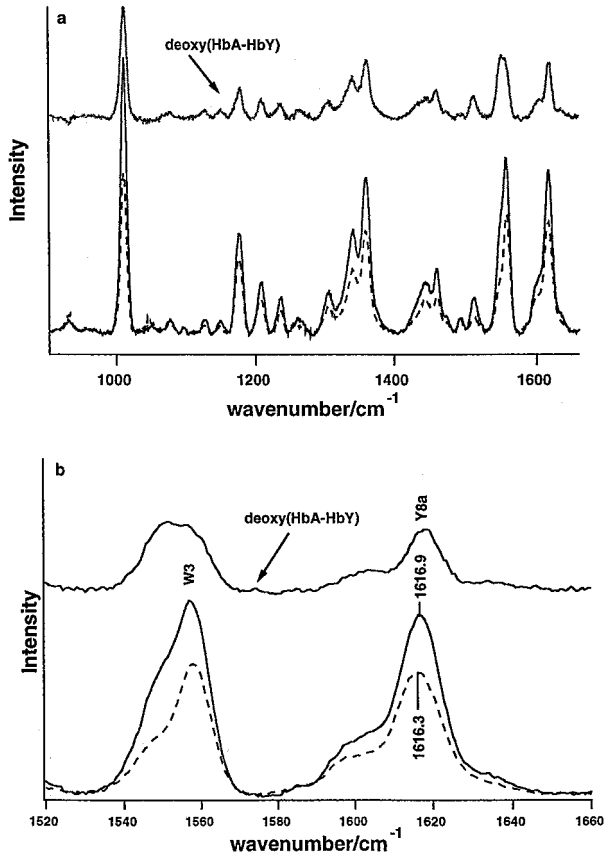

FIGURE 8: (a) Comparison of the UV resonance Raman spectra of deoxyHbA (solid line) and deoxyHbY (dashed line) utilizing spectra shown in Figures 5 and 6. A blowup of the W3 and Y8a bands and the corresponding expanded difference spectrum, deoxyHbA − deoxyHbY, are shown in (b).

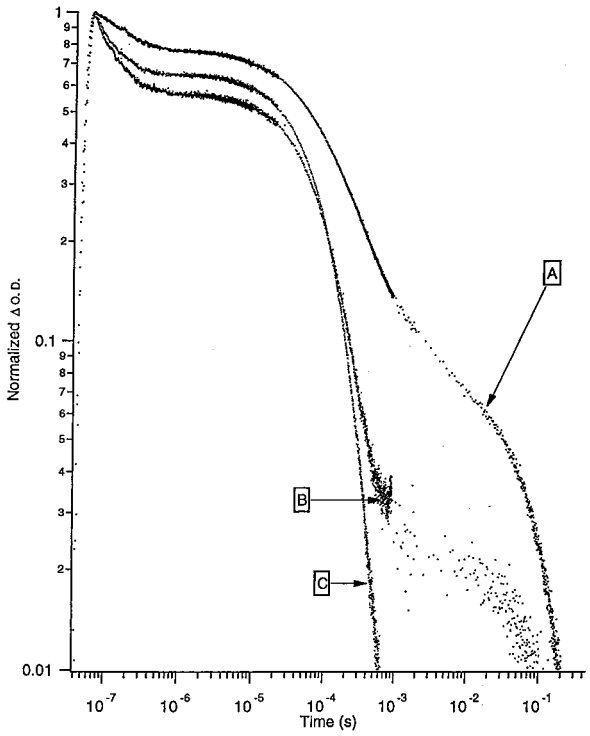

FIGURE 9: Ligand rebinding after photodissociation using a 7 ns 532 nm excitation pulse. The data are displayed as a log−log plot of optical density change (proportional to the population of photoproduct) versus time. (A) is the rebinding for COHbA plus 0.3 M highly pure sodium perchlorate. (B) is the rebinding for COHbY plus 0.3 M highly pure sodium perchlorate. (C) is the rebinding for COHbY without perchlorate. The sample temperature for curves A and B was 20 °C, whereas the temperature for curve C was at 25 °C. All the solutions are fully saturated with CO and are in 0.05 M Hepes, pH 7.5.

slower phases occurring after the microsecond plateau are the recombinations derived from CO in the solvent (the solvent is saturated with CO). It can be seen that in the presence of perchlorate (curve B), the yield and effective overall rate for the geminate recombination are greater for HbY than for HbA (curve A). At low ionic strength, the difference in the geminate yield between the two hemoglobins is substantially reduced, primarily as a result of an enhancement for the yield in HbA. Thus, the kinetic trace for HbA at low ionic strength resembles quite closely that of HbY (curve C) but with an important difference. As can be seen in the figure, HbY at low ionic strength (curve C) does not exhibit the slow millisecond solvent rebinding phase that is always observed for HbA (albeit with solution-dependent amplitudes, vide infra). Both hemoglobins show an increase in the geminate yield with a decrease in temperature (data not shown).

Two distinct bimolecular solvent recombination phases are seen for HbA. The addition of perchlorate increases the amplitude of the slower phase relative to the faster phase. In the presence of 0.3 M perchlorate or 0.1 M NaCl (not shown), the apparent rate of the fast solvent phase is faster for HbY. In 0.05 M Hepes alone, HbY exhibits only a single solvent phase, which is comparable to the faster solvent phase of HbA. In the presence of perchlorate or at higher temperatures, HbY exhibits a slow solvent phase as well, but with a markedly reduced amplitude compared to HbA (less than 5% of the total population). At high ionic strength, it is apparent that the fast solvent phase of HbY is faster than the corresponding fast solvent phase of HbA.

DISCUSSION

Functional Properties. Earlier studies (*1*) established that HbY compared to HbA has a much enhanced oxygen affinity (as reflected in its P50) and a near-complete absence of cooperativity. In contrast to HbA, HbY exhibits a very slight decrease in oxygen affinity and increase in cooperativity upon addition of the allosteric effector IHP. The overall oxygen affinity as measured using P_{50} values and the degree of cooperativity as measured by n, the Hill coefficient, do not provide detailed insight into the molecular mechanism responsible for the altered reactivity. This statement follows from the fact that the above two measurements are reflective of a ligand-binding dependent equilibrium involving multiple conformations. A more appropriate approach is to focus on measures of reactivity that can be associated with each of these specific conformations.

The local heme environment of the protein species that is generated upon ligand dissociation modulates geminate recombination in hemoglobins (*37*−*43*). In hemoglobin, where the local tertiary structure of the photoproduct does not begin to relax until at least tens of nanoseconds after photodissociation (*33*, *40*, *41*), the initial local environment influencing geminate rebinding is very nearly identical to that of the starting ligand-bound species (with the exception of a very rapid and very local iron out-of-plane motion) (see

ref *42* for a discussion of this point). A time-dependent increase in the potential energy barrier controlling iron−ligand bond formation, due to tertiary relaxation of the hemoglobin photoproduct on the time scale of geminate rebinding, can be expected to slow the rate of rebinding as initially proposed by Friedman and co-workers (*40, 43*) and more recently verified by Eaton and co-workers (*41*). Such a process has been used to explain the inverse temperature effect in photodissociated carboxy myoglobin (*44*). Thus, geminate rebinding is a measure of ligand binding reactivity that can be directly associated with the tertiary structure of the initial photoproduct and its subsequent evolution.

There are three general mechanisms for protein control of geminate recombination (for a review, see ref *45*). The first is the influence of the heme pocket architecture on the dynamics of the dissociated ligand. Residues can either block or facilitate escape of the dissociated ligand from the heme pocket. Similarly, residues can facilitate or block access of the ligand to the iron. This mechanism would also include the steric influence of internal waters and the impact of local docking sites on the trajectories for both ligand escape and ligand rebinding. Studies on mutant myoglobins have shed considerable light on this aspect of control. The second mechanism is the electrostatic influence of the local environment. This would include the influence of the local polarity of the heme pocket on the stability of iron−ligand transition states, localized internal waters, and possibly dissociated ligands. With respect to the transition state, this mechanism of control arises largely from the potential stabilization by distal heme pocket residues of the dipole created when the ligand binds to the heme iron. Note that these first two mechanisms are derived primarily through distal heme pocket influences whereas the third, described in detail below, is based on the interaction of the heme with the proximal residue that is covalently coordinated to the heme iron.

This last mechanism of control is proximal strain which refers to the energy expenditure against the protein upon ligand binding derived from the movement of the iron into the heme plane. Contributions to the stability of the transition state arise from the degree to which the iron moves toward a more planar position for the particular transition state associated with the binding of a particular ligand (*14, 42, 46*). For ligands such as CO that have product-like transition states, the formation of the transition state is expected to be accompanied by a substantial movement of the iron toward the heme plane and thus be especially vulnerable to proximal strain.

Protein modulation of proximal strain occurs through the iron−proximal histidine linkage. Conformational changes, such as shifts in the F helix, that alter the orientation (e.g., tilt and azimuthal angle) of the proximal histidine with respect to the heme influence the ease with which the iron can move into the heme plane. Also included in this category are alterations in the iron−proximal histidine bond strength induced through changes in the hydrogen bonding of the δ-nitrogen proton to residues within the proximal heme pocket.

The variation in geminate yield in hemoglobins as a function of both quaternary and tertiary structure has been attributed largely to the proximal strain mechanism. This conclusion stems in part from X-ray data and from correlations between spectroscopic indicators of proximal strain and variation in both geminate rebinding (*23, 38, 42, 46*) and other measures of ligand reactivity (*23, 48, 49*). In addition, the absence of sizable changes in the polarity-sensitive CO and Fe−C stretching frequencies for carboxy derivatives of hemoglobin in various quaternary and tertiary structures (J. Holt and G. Ackers, private communication) argues against the second mechanism as a major factor in hemoglobin reactivity. In contrast, the large variation in the geminate yields and rates in mutated myoglobins (*45*) and several invertebrate hemoglobins (*50*) has been directly linked to the first two mechanisms.

The present study reveals that the geminate phase for COHbY has a higher yield and faster rate than for COHbA under comparable conditions of high ionic strength. It can be seen in Figure 9 that the geminate phase terminates with an onset of a plateau in the kinetics that is followed by the solvent phase rebinding starting at approximately 100 μs. For HbA, the solvent phase kinetics are composed of two major components. The faster and slower components are ascribed to ligand rebinding to high-affinity (R) and low-affinity (T) species, respectively (*51*). Since the initial photoproduct population is entirely R state for HbA, the observation of the slower solvent phase is indicative of a quaternary switch from R to T for some fraction of the photoproduct population. The solvent phase rebinding kinetics for HbY differ from those of HbA in that the slow phase either is not occurring or is greatly reduced possibly due to a more rapid fast phase in HbY. A detailed analysis of the kinetics for both hemoglobins is made difficult by virtue of the fact that at the onset of the solvent phase rebinding there is an uncharacterized mix of partially liganded species resulting from partial recombination during the geminate phase.

In the following discussion, an attempt will be made to use the spectroscopic results to elucidate the molecular origins of the kinetic differences in the two ligand rebinding processes in terms of structures and conformational stability.

The 10 ns Photoproduct: Band III. Both band III and the Soret-enhanced resonance Raman spectra are essentially the same for HbA*(10 ns) and HbY*(10 ns). Band III is a charge-transfer absorption band arising from a porphyrin π to iron d orbital. The peak position of this charge-transfer transition is responsive both to proximal strain, as reflected in the frequency of the ν(Fe−His) mode, and to the polarity of the distal heme pocket (*13, 21, 22*). Thus, these spectroscopic results indicate that the heme and the heme environment for both photoproducts are very similar at early times. The frequencies and peak positions are all consistent with an R-like photoproduct at 10 ns after photodissociation. Based on these result, one might anticipate identical geminate phases for the two proteins.

The 10 ns Photoproduct: The Visible Resonance Raman Spectrum. The photoproduct spectra of COHbA and COHbY at 10 ns (Figure 5) are identical under the solution conditions used in this study. Both spectra show the features in the region of the propionate-sensitive bands (300−400 cm^{-1}) that are indicative of a heme environment that still retains molecular memory of the initial liganded conformation (*40, 52*). Most significant from the perspective of ligand binding reactivity is the conformation-specific 214−230 cm^{-1} frequency of ν(Fe−His), the iron−proximal histidine stretching mode.

The iron−proximal histidine stretching mode has been extensively studied and characterized (*23*, *33*, *42*, *43*, *48*, *49*, *53*−*60*). It is observed for both stable and transient forms of ferrous five-coordinate Hb but not for six-coordinate species. Studies on both mutants and iron−metal and valency hybrid Hbs reveal that the frequency of this subunit-sensitive band varies systematically with tertiary and quaternary structure (*23*, *24*, *42*, *43*, *46*, *54*, *57*, *59*, *60*).

For the α subunit, the frequency of ν(Fe−His) increases from ∼205 to 229 cm^{-1} in going from deoxy T to R* (photodissociated liganded R), whereas for the β subunit the frequency starts at ∼217 cm^{-1} for deoxy T and also ends at 229 cm^{-1} for R*. The observed composite frequency for deoxy T is ∼214 cm^{-1}. This frequency increases to ∼217−222 cm^{-1} for T* (photoproduct T) which is similar in frequency to those species that have been assigned as deoxy R or very unstable deoxy T. Reducing the pH to below 7 and adding IHP decrease the frequency of R* from 229 to 225 cm^{-1} (*23*, *40*, *59*). It is noteworthy that, in the present study, the frequency of ν(Fe−His) for Hb*(10 ns) from both proteins at pH 7.4 decreases from 229 to 225 cm^{-1} in going from 0.05 M Hepes buffer to 0.1 M Tris plus 0.1 M NaCl (data not shown). It must be noted that for the intermediate frequencies associated with species such as deoxy R and T* there is both considerable variability in the frequency and also considerable ambiguity with regard to the explicit nature of the quaternary state. A recent study (*23*) on a series of β37 mutants of HbA reveals that within the boundaries of the T quaternary state, there is a range of accessible frequencies for ν(Fe−His) for the deoxy derivatives. Both this study and the finding that there are different frequencies for ν(Fe−His) for the deoxy and photoproduct forms of both R and T are reflective of the conformational plasticity associated with the tertiary structures that can be accessed for a given quaternary state.

Functional Implication of the Tertiary Relaxation Rate Difference. The present study as well as earlier studies (*18*, *20*) show that for HbA*(*t*), band III relaxes toward the equilibrium deoxy value over a wide range of time scales that start on the tens of nanosecond time scale and end after tens of microseconds. Similar relaxation kinetics have been observed using time-resolved visible (*30*, *35*) and UV resonance Raman (*30*) as well as Soret band based transient absorption (*33*, *40*). These relaxations have been linked to a progressive increase in the potential energy barrier for ligand rebinding which makes it progressively less likely for ligand rebinding to occur (*40*−*43*, *46*). Whereas for HbA* under conditions of moderate to high ionic strength there is substantial conformational relaxation over the time scale of the geminate phase, there is very little relaxation observed on this time scale for HbY*. The difference in the degree of relaxation implies that although both photoproducts start out with similar heme environments, the local heme environments progressively diverge with time after ligand dissociation. The functional implication is that the barrier for rebinding should remain lower for HbY, thus resulting in a greater geminate yield, as is observed. Under conditions of lower ionic strength, relaxation of HbA* slows and the difference between the two proteins with respect to geminate recombination diminishes.

The reduced level of relaxation for HbY* for times beyond 50 μs also accounts for both the faster solvent phase R state rebinding and the absence or reduction of the slower T state component. The population of photoproduct at the onset of the solvent phase is still substantially unrelaxed as reflected in the 764 nm peak position of band III for the ligand-free hemes (Figure 1). Thus, the average rebinding barrier height for this population should be lower than for the more relaxed corresponding population associated with HbA* (761 versus 764 nm). The R to T switching time for HbA* is on the order of a few tens of microseconds. In contrast, HbY* does not show any indication of T state formation on these time scales which is consistent with the loss or reduction of the slow millisecond solvent phase for ligand recombination.

The substantial difference in the relaxation properties of HbA* and HbY* can account for differences in the ligand rebinding kinetics. The origin of this relaxation difference is unclear. Both HbA*(10 ns) and HbY*(10 ns) appear similar with respect to the local heme environment; thus, difference in the relaxation rates must originate from conformational differences away from the local heme environment. Thus, it is important to evaluate protein conformational differences between COHbA and COHbY beyond the environs of the heme.

Although HbY* does not relax on the time scale of our measurements, the visible Raman and band III studies reveal that a distinct deoxy conformation exists for HbY that is readily distinguishable from both HbY* and deoxyHbA. Thus, the question regarding the origin of the HbY* − HbA* relaxation difference must also address the nature of this deoxyHbY conformation. The slow relaxation of HbY* implies that this distinct deoxyHbY conformation is not as easily accessed from HbY* as are either the deoxy R or the deoxy T conformations from HbA*.

UV Resonance Raman Spectra: COHbA versus COHbY. Excitation with 229 nm light results in a Raman spectrum from hemoglobins that is composed primarily of contributions from tyrosine and tryptophan. This relatively new spectroscopy can be used to characterize the environment, the hydrogen bonding patterns, and in some cases the stereochemistry of specific aromatic residues as a function of ligand binding.

A comparison between deoxyHbA and COHbA (Figure 5), as well as T and R forms of metHb, reveals R − T differences in several of the tryptophan modes that are clearly attributable to Trp β37 (*28*−*30*, *62*). This tryptophan forms the key contacts associated with the flexible joint region of the $\alpha_1\beta_2$ interface. With 229 nm excitation, the W3 Raman band at ca. 1557 cm^{-1} has a low-frequency shoulder at ∼1547 cm^{-1} that has been assigned to Trp β37 based on a comparison between HbA and mutants lacking Trp β37 (30). The main portion of the W3 Raman band at 1557 cm^{-1} arises from Trp α14 and Trp β15, each on the A helix of their respective subunit. Variation in the intensity of the α14,β15 component of the W3 band has been attributed to changes in the packing of the A and E helices. The packing modulates the hydrogen bond strength between the tryptophan on the A helix and its hydrogen bonding partner on the E helix (*25*, *28*−*30*, *63*).

The frequency of the W3 band correlates with the dihedral angle about the bond connecting the indole ring to the C_β atom of the tryptophan side chain (*27*), whereas the intensity changes are due to changes in H-bonding or in the local dielectric (*25*, *28*−*30*, *64*, *67*). For HbA, the T to R transition

is associated with a decrease in the intensity of the 1547 cm^{-1} β37 shoulder with only minimal change in the relative intensity of the main 1557 cm^{-1} portion of the W3 band.

The present study shows that the CO derivative of HbY has the same β37 environment (hinge or flexible joint region of the $\alpha_1\beta_2$ interface) as COHbA (see Figure 7). This result indicates that COHbY has an R-like conformation in the flexible joint or hinge region of the $\alpha_1\beta_2$ interface. This region has been shown through both X-ray crystallography (*65*) and Raman spectroscopy (*23*) to be connected to the proximal environment surrounding the hemes. The identical β37 environment is consistent with both the frequency of ν(Fe−His) (Figure 4) and the peak wavelength of band III being the same for the photoproducts of COHbA and COHbY (Figure 1c,d) prior to the onset of relaxation. Similarly, the identical position and intensity for the 1557 cm^{-1} main portion of the W3 band is indicative of a similar packing arrangement for the A and E helices of the two liganded derivatives.

The R − T frequency difference in the tyrosine Y8a band at ca. 1615 cm^{-1} for HbA (229 nm excitation) (Figure 5) has been attributed (*24, 28*−*33, 64, 66*) to the loss of the H-bond between Tyr α42 and Asp β99 in going from T to R. At least part of that R to T state frequency change has been shown to arise from other residues (Asp α94 and Arg β40) contributing to a positive electrostatic field near α42 in the T state (*66*). Changes in the intensity of this Raman band have been tentatively attributed to changes in the hydrogen bonding of the penultimate tyrosines (*24*). Support for these assignments comes from our recent study on the Yα42A mutant (Juszczak, Peterson, and Friedman, unpublished results). This mutant, which remains highly cooperative despite the absence of the Tyr α42−Asp β99 hydrogen bond in the T state, exhibits the usual deoxy versus CO changes in the ν(Fe−His) (of the visible RR spectrum), in the W3 band (of the UVRR spectrum), and in the T − R difference band at 1511 cm^{-1} (of the UVRR spectrum). As expected (due to the absence of Tyr α42), a ligand-dependent frequency shift is not observed for Y8a in the UVRR spectrum of the Yα42A mutant. Instead, Y8a decreases in intensity in going from the deoxy to the CO derivative. This decrease is consistent with a weakening of the hydrogen bond between penultimate tyrosines and the FG5 valines upon switching from T to R. A similar conclusion was reached in an earlier study (*24*) on a cooperative double mutant variant of Hb Kempsey (Dβ99N; Yα42D).

An assessment of the changes in Y8a for the HbY/HbA comparisons is difficult and not straightforward due to the additional tyrosine in HbY. It can be seen (Figure 7) that Y8a is at approximately the same frequency for COHbA (1615.9 cm^{-1}) and COHbY (1615.3 cm^{-1}). The similar frequencies argue in favor of a very similar environment for the α42 tyrosines in the switch region of the $\alpha_1\beta_2$ interface. From Figure 7 it is not clear how much of the Y8a intensity difference is due to the additional tyrosine or to changes in the tyrosine hydrogen bonding interactions. The intensity increase is close to what is expected if the two additional tyrosines contribute to Y8a with comparable scattering intensity as the other contributing tyrosines.

The difference spectrum between COHbA and COHbY contains one unexplainable feature. Whereas there are very few difference features associated with most of the tryptophan bands, there is a distinct peak for W16 at ∼1010 cm^{-1} indicative of greater intensity for the normalized COHbA sample. If the tryptophans in the two samples contribute identically to their respective spectra (i.e., the environment about each tryptophan is identical for the two samples), then one would expect cancellation of all the tryptophan peaks in the difference spectrum. The failure of W16 to cancel out may be due to the greater solvent dependence of this mode compared to W3 as observed by Chi and Asher (*57*) in a myoglobin unfolding experiment. If so, the results are consistent with a difference in the solvent exposure of the tryptophans in the two CO samples. Overall, the UV resonance Raman spectrum of COHbY indicates a conformation that is very similar to that of solution phase COHbA.

Spectroscopic Characterization of DeoxyHbY. The peak positions of both band III and ν(Fe−His) for deoxyHbY are between those values associated with deoxyHbA and HbA*. These peak positions for deoxyHbY are consistent with either a deoxy R conformation or a highly destabilized deoxy T conformation (*23*).

Studies (*23, 65, 68*) on β37 mutants of HbA reveal that the T quaternary state can accommodate a family of tertiary structures. This family comprises a range of proximal heme environments correlated with a systematic distribution of conformations at the hinge region of the $\alpha_1\beta_2$ interface and at the nearby C terminus of α subunits which includes the packing of the α145 penultimate tyrosine. The near-IR absorption and visible resonance Raman spectroscopic values obtained for deoxyHbY are consistent with a highly destabilized deoxy T state conformation which is likely similar to that of deoxy Wβ37E (*23*).

Similarly, one might argue that the "midpoint" spectroscopic values for deoxyHbY are also consistent with a deoxy R state conformation. Indeed, both the previously described thermodynamics and the β93 sulfhydryl reactivity measurements suggest an R-like conformation for the deoxy form of HbY (*1*).

Spiro and co-workers (*29*−*33, 64*) have claimed that the spectral signature of the deoxy R species is a distinctive UV resonance Raman spectrum. This spectrum displays reduced intensities with an absence of frequency shifts for most of the tyrosine and tryptophan bands when compared to the corresponding spectrum from the fully liganded R state species. The deoxyHbY minus COHbY UV Raman difference spectrum (Figure 6) is strikingly reminiscent of the difference spectra assigned by Spiro and co-workers to deoxy R minus liganded R. Given the similarity between the COHbA and COHbY spectra, it is reasonable to conclude that the HbY difference spectrum is also reflective of this same liganded R − deoxy R comparison. The most striking features in the HbY difference spectrum are the strong negative bands for the W3 and Y8a bands. These have been attributed to, respectively, a weakening in the deoxy R species of the hydrogen bonding both between the A helix tryptophans and their bonding partners on the E helix and between the penultimate tyrosines and the FG5 valines (*29*−*33, 64*). The packing of A and E helices has been linked to the status of the H helix which provides a scaffolding for the overall packing of these and other helices (*64*).

The HbY difference spectrum (Figure 7) does differ from the typical deoxy R minus liganded R difference spectrum

in that the normally observed negative feature associated with W16 at 1013 cm^{-1} is now a weak positive feature in the HbY difference. This can be attributed to the reduced intensity of this band in the COHbY spectrum as described above. It may be that the weak positive feature at W16 is indicative of some degree of T-like character either in the deoxy population (i.e., some molecules in solution are more T-like) or in a conformation in which some T state interactions are contributing. Support for this idea comes from the observation that in going from COHbY to deoxyHbY, Y8a upshifts by 1 cm^{-1}, which is a reduced version of what occurs for HbA upon switching from R to T. The larger shift in HbA has been attributed to the R to T conformational changes at α42 tyrosine (vide supra). The appearance of a small population of slowly rebinding HbY after photodissociation of the carboxy derivative (Figure 9B) is also indicative of HbY being capable of accessing a T-like structure, albeit with difficulty.

The spectroscopic data presented here, in conjunction with the absence for HbY of an alkaline Bohr effect and the high reactivity rate of the β93 sulfhydryl toward PDS for the deoxy derivative (*1*), are consistent with deoxyHbY existing in solution predominantly in an R-like conformation. Thus, this deoxy conformation should manifest the usual disruption of the T state hydrogen bonding network associated with the C terminus His β146. The UV Raman data from deoxyHbY provide evidence for a disruption of the hydrogen bond between the penultimate tyrosines and the FG5 valines (β subunits) that is present both for the liganded R conformation and for the deoxy T conformation. Thus, in some sense this deoxy R conformation is more of a transition state structure in which at least some of the interactions that maintain the two end point structures (deoxy R and liganded R) are loosened. This conclusion is consistent with the time evolution of the UVRR spectrum of HbA* which shows the appearance of this intermediate spectrum occurring as the liganded R state spectrum decays and before the appearance of T state markers (*29*−*31*, *33*). The "looseness" of this structure is also consistent with the relative ease with which the frequency of ν(Fe−His) can be shifted with ionic strength for deoxyHbY (Figure 4).

A Possible Origin for the Reduced Tertiary and Quaternary Relaxations in the HbY Photoproduct. The Y quaternary structure reported for COHbY in the crystal state, which partially resembles the low-salt R2 structure of HbA (*3*), has conformational parameters that place it within the R state family of structures (A. Arnone, personal communication). One feature of this structure that may account for the diminished tertiary relaxation in HbY* is the altered positioning of the β145 tyrosine. In COHbY, the β145 tyrosine side chain is rotated 180° about the torsion angle χ_1 from its normal liganded R state position and therefore no longer hydrogen bonds with β98 Val (*2*). This particular hydrogen bond is maintained in both the deoxy T and liganded R structures of HbA (*69*). Janin and Wodak (*9*) hypothesized, on the basis of an analysis of the crystal structure, that the new position of the β145 side chain represents a tightly packed and stable configuration for the tyrosine side chain. If for COHbY the tyrosine side chain is highly stabilized in this alternate position, then a disengagement of the side chain would be necessary in order to form either the deoxy R or the deoxy T conformation. The deoxy R conformation has the penultimate tyrosines disengaged from the cleft, whereas the deoxy T state has the penultimate tyrosines tightly packed but in a different cleft. It is therefore plausible that the slow HbY* relaxation kinetics are a direct result of a high potential energy barrier associated with the shift of the β145 side chain from the stable Y state position to either the intermediate transition state deoxy R position or the deoxy T state position. Previous studies (*70*, *71*) have shown that the penultimate tyrosine and its interactions with neighboring residues contribute to the potential energy barrier separating the R and T state species.

The absence of a clear spectroscopic indication of a fully formed T state for the deoxy derivative argues in favor of a large destabilization of the T structure due to the altered interactions arising from the Dβ99Y mutation. Surprisingly, the inability to form the T state α42 to β99 hydrogen bond is not by itself responsible for this destabilization. This statement follows since the deoxy derivative of the Yα42A mutant yields a normal deoxy T visible and UV resonance Raman spectrum (Juszczak, Peterson, and Friedman, unpublished results) and its crystal structure is clearly T state (A. Arnone, personal communication). Furthermore, the UV resonance Raman spectrum of deoxyHb Kempsey (Dβ99N) is consistent with a T state structure albeit with weakened interactions (T. Spiro, personal communication).

Origin of the Quaternary Enhancement Effect: Role of Tertiary Relaxation. In an earlier study (*68*) it was shown that enhancement of ligand binding in going from the separated αβ dimers to the R state Hb tetramer (quaternary enhancement) is at least partially manifested in an increase in the geminate yield of the liganded tetrameric hemoglobin over that of the corresponding αβ dimers. The conformational basis for this enhancement was ascribed to the enhanced reduction in proximal strain in the nanosecond photoproduct of the R state tetramer relative to the corresponding species derived from the dimer (*23*). Spectroscopically, this enhancement of the proximal environment by the tetramer is evident from the increased frequency (225−230 cm^{-1}) of ν(Fe−His) in the R (R2, Y) state tetrameric photoproduct relative to the dimer or isolated chains (∼222−225 cm^{-1}). Similarly, the quaternary constraint of the T state tetramer is reflected in part through a reduced geminate yield for the T state photoproduct (*37*−*39*, *46*, *61*) and an enhancement of proximal strain as seen (*24*, *39*, *42*, *46*, *56*) in a reduced frequency for ν(Fe−His) (∼204−222 cm^{-1}). Thus, relative to the dimer and the isolated chains, the T state tetramer enhances and the liganded R state tetramer diminishes proximal strain.

The 10 ns photoproducts of COHbA and COHbY yield similar frequencies for ν(Fe−His) (Figure 4), and as a consequence, one might anticipate a similar degree of quaternary enhancement. The thermodynamic data of Ackers and co-workers indicate that HbY in a buffer having a moderately high ionic strength (0.1 M chloride) has a substantially larger quaternary enhancement effect compared to HbA and other β99 mutants. In the present study, we see that at high ionic strength the geminate yield for COHbA is noticeably reduced compared to COHbY, which is consistent with the greater degree of quaternary enhancement for HbY. Although both photoproduct species start off with comparable reductions in proximal strain as reflected in the high frequency of ν(Fe−His), the band III time-resolved study

indicates that the relaxation of the initial photoproduct conformation is much slower for HbY. The result of a slowed relaxation is that over the time course of the geminate rebinding phase and out to the onset of the first bimolecular solution phase rebinding, the population of HbY photoproduct will contain a larger fraction of conformations having the enhanced proximal environment. It is anticipated that under conditions where the relaxation of the HbA photoproduct also slows down [e.g., low ionic strength (J. Huang and J. M. Friedman, unpublished results) or high pH (*40*)], the difference in the geminate yield for the two hemoglobins would be reduced, as appears to be the case from this study. Similarly, the quaternary enhancement effect is in general maximized under conditions of low ionic strength (*5*) and high pH (G. Ackers, personal communication). It is reasonable to attribute this solvent-induced maximization of the quaternary enhancement effect to a combination of the static proximal effect and the reduction in relaxation rates, both of which reflect a stabilization of the conformations having the most favorable proximal heme pocket parameters with respect to ligand binding.

CONCLUSIONS

The spectroscopic results of this study indicate that in solution, COHbY has many of the R-like conformational features associated with the liganded HbA. The deoxy derivative of HbY exhibits spectroscopic properties that are similar to those attributed to the deoxy R state conformation. Many of the ligand rebinding properties observed for photodissociated COHbY are explainable based on the observation that the initial photoproduct conformation relaxes very slowly compared to the corresponding photoproduct derived from COHbA. A proposed explanation for the slow relaxation of the HbY photoproduct is based on an alternative and highly stable position for the β145 tyrosine in COHbY (vis à vis in COHbA).

The spectroscopic and geminate rebinding results of this study indicate that the quaternary enhancement effect associated with the high-affinity forms of tetrameric hemoglobins originates from static and dynamic factors. Geminate rebinding in the tetramer can be increased not only via the tetramer-induced enhancement of the proximal heme pocket environment but also from the tetramer-modulated relaxation of the initial liganded conformation after ligand dissociation.

ACKNOWLEDGMENT

We thank Drs. Ackers and Holt for providing samples of HbY and helpful technical information, Drs. Acharya and Hirsch for providing assistance with obtaining and purifying samples of HbA, Dr. B. Manjula for determining the purity of HbY samples, Drs. Acharya, Arnone, and Kavanaugh for helpful discussions, and Dr. Spiro for sharing and discussing preliminary results on Hb Kempsey.

REFERENCES

1. Doyle, M. L., Lew, G., Turner, G. J., Rucknagel, D. and Ackers, G. K. (1992) *Proteins: Struct., Funct., Genet. 14*: 351−362.
2. Smith, F. R., Lattman, E. E., and Carter, C. W. (1991) *Proteins: Struct., Funct., Genet. 10*, 81−91.
3. Silva, M. M., Rogers, P. H., and Arnone, A. (1992) *J. Biol. Chem. 267*, 17248−17256.
4. Perutz, M. F. (1990) *The Mechanism of Cooperativity and Allosteric Regulation in Proteins*, Cambridge University Press, Cambridge, U.K.
5. Ackers, G. K. (1998) *Adv. Protein Chem. 51*, 185−253.
6. Schumacher, M. A., Dixon, M. M., Kluger, R., Jones, R. T., and Brennan, R. G. (1995) *Nature 375*, 84−87.
7. Schumacher, M. A., Zheleznova, E. E., Poundstone, K. S., Kluger, R., Jones, R. T., and Brennan, R. G. (1997) *Proc. Natl. Acad. Sci. U.S.A. 94*, 7841−7844.
8. Bucci, E., Fronticelli, C., and Gryczynski, Z. (1991) *Biochemistry 30*, 3195−3199.
9. Janin, J., and Wodak, S. J. (1993) *Proteins: Struct., Funct., Genet. 15*, 1−4.
10. Srinivasan, R., and Rose, G. D. (1994) *Proc. Natl. Acad. Sci. U.S.A. 91*, 11113−11117.
11. Eaton, W. A., Hanson, L. K., Stephens, P. J., Sutherland, J. C., and Dunn, J. B. R. (1978) *J. Am. Chem. Soc. 100*, 4991−5003.
12. Iizuka, T., Yamamoto, H., Kotani, M., and Yonetani, T. (1974) *Biochim. Biophys. Acta 371*, 126−139.
13. Chavez, M. D., Courtney, S. H., Chance, M. R., Kiula, D., Nocek, J., Hoffman, B. M., Friedman, J. M., and Ondrias, M. R. (1990) *Biochemistry 29*, 4844−4852.
14. Ahmed, A. M., Campbell, B. F., Caruso, D., Chance, M. R., Chavez, M. D., Courtney, S. H., Friedman, J. M., Iben, I. E. T., Ondrias, M. R., and Yang, M. (1991) *Chem. Phys. 158*, 329−351.
15. Campbell, B. F., Chance, M. R., and Friedman, J. M. (1987) *Science 238*, 373−376.
16. Agmon, N. (1988) Biochemistry *27*, 3507−3511.
17. Srajer, V., and Champion, P. M. (1991) *Biochemistry 30*, 7390−7402.
18. Sassarole, M., and Rousseau, D. L. (1987) *Biochemistry 26*, 3092−3098.
19. Huang, J., Leone, M., Boffi, A., Friedman, J. M., and Chiancone, E. (1996) *Biophys. J. 70*, 2924−2929.
20. Huang, J., Ridsdale, A., Wang, J., and Friedman, J. M. (1997) *Biochemistry 36*, 14353−14365.
21. Kiger, L., Stetzkowsky-Marden, F., Poyart, C., and Marden, M. C. (1995) *Eur. J. Biochem. 228*, 665−668.
22. Christian, J. F., Unno, M., Sage, J. T., Champion, P. M., Chien, E., and Sligar, S. G. (1997) *Biochemistry 36*, 11198−11204.
23. Peterson, E. S., and Friedman, J. M. (1998) *Biochemistry 37*, 4346−4357.
24. Huang, S., Peterson, E. S., Ho, C., and Friedman, J. M. (1997) *Biochemistry 36*, 6197−6206.
25. Juszczak, L. J., Hirsch, R. E., Nagel, R. L., and Friedman, J. M. (1998) *J. Raman Spectrosc*. (in press).
26. Gottfried, D. S., Peterson, E. S., Sheikh, A. G., Wang, J., Yang, M., and Friedman, J. M. (1996) *J. Phys. Chem. 100*, 12034−12042.
27. Austin, J. C., Jordan, T., and Spiro, T. G. (1993) *Biomolecular Spectroscopy*, Part A, Chapter 2, p 55.
28. Hu, X., and Spiro, T. G. (1997) *Biochemistry 36*, 15701−15712.
29. Su, C., Park, Y. D., Liu, G., and Spiro, T. G. (1989) *J. Am. Chem. Soc. 111*, 3457−3459.
30. Rodgers, K. R., Su, C., Subramaniam, S., and Spiro, T. G. (1992) *J. Am. Chem. Soc. 114*, 3697−3709.
31. Rodgers, K. R., and Spiro, T. G. (1994) *Science 265*, 1697−1699.
32. Mukerji, I., and Spiro, T. G. (1994) *Biochemistry 33*, 13132−13139.
33. Jayaraman, V., Rodgers, K. R., Mukerji, I., and Spiro, T. G. (1995) *Science 269*, 1843−1848.
34. Alpert, B., El Mohsni, S., Lindqvist, J., and Tfibel, F. (1979) *Chem. Phys. Lett. 64*, 11−16.
35. Duddell, D. A., Morris, R. J., and Richards, J. T. (1979) *J. Chem. Soc., Chem. Commun*., 75−76.
36. Friedman, J. M., and Lyons, K. B. (1980) *Nature 284*, 570−572.
37. Murry, L. P., Hofrichter, J., Henry, E. R., Ikeda-Saito, M., Kitagishi, K., Yonetani, T., and Eaton, W. A. (1988) *Proc. Natl. Acad. Sci. U.S.A. 85*, 2151−2155.

38. Friedman, J. M., Scott, T. W., Fisanick, G. J., Simon, S. R., Findsen, E. W., Ondrias, M. R., and MacDonald, V. W. (1985) *Science 229*, 187−190.
39. Friedman, J. M., Scott, T. W., Stepnoski, R. A., Iketda-Saito, M., and Yonetani, T. (1983) *J. Biol. Chem. 258*, 10564−10572.
40. Scott, T. W., and Friedman, J. M. (1984) *J. Am. Chem. Soc. 106*, 5677−5687.
41. Henry, E. R., Jones, C. M., Hofrichter, J., and Eaton, W. A. (1997) *Biochemistry 36*, 6511−6528.
42. Friedman, J. M. (1994) *Methods Enzymol. 232*, 205−231.
43. Friedman, J. M. (1985) *Science 228*, 1273−1280.
44. Agmon, N., and Hopfield, J. J. (1983) *J. Chem. Phys. 79*, 2042−2053.
45. Olson, J. S., and Phillips, G. N. (1996) *J. Biol. Chem. 271*, 17593−17596.
46. Rousseau, D. L., and Friedman, J. M. (1988) In *Biological Application of Raman Spectroscopy* (Spiro, T. G., Ed.) Vol. III, pp 133−215, Wiley and Sons, New York.
47. Kitagawa, T. (1992) *Prog. Biophys. Mol. Biol. 58*, 1−18.
48. Kitagawa, T. (1988) In *Biological Application of Raman Spectroscopy* (Spiro, T. G., Ed.) Vol. III, pp 97−131, Wiley and Sons, New York.
49. Matsukawa, S., Mawatari, K., Yoneyama, Y., and Kitagawa, T. (1985) *J. Am. Chem. Soc. 107*, 1108−1116.
50. Peterson, E. S., Huang, S., Wang, J., Miller, L. M., Vidugiris, G., Kloek, A. P., Goldberg, D. E., Chance, M. R., Wittenberg, J. B., and Friedman, J. M. (1997) *Biochemistry 36*, 13110−13121.
51. Antonini, E., and Brunori, M. (1971) *Hemoglobin and Myoglobin in their Reactions with Ligands*, North-Holland, New York.
52. Jayaraman, V., and Spiro, T. G. (1996) *Biospectroscopy 2*, 311−316.
53. Argade, M., Sassaroli, P. V., Rousseau, D. L., Inubushi, T., Ikeda-Saito, M., and Lapidot, A. (1984) *J. Am. Chem. Soc. 106*, 6593−6596.
54. Nagai, K., and Kitagawa, T. (1979) *Proc. Natl. Acad. Sci. U.S.A. 77*, 2033−2037.
55. Nagai, K., Kitagawa, T., and Morimoto, H. (1980) *J. Mol. Biol. 136*, 271−289.
56. Friedman, J. M., Rousseau, D. L., Ondrias, M. R., and Stepnoski, R. A. (1982) *Science 218*, 1244−1246.
57. Ondrias, M. R., Rousseau, D. L., Kitagawa, T., Ikeda-Saito, M., Inubushi, T., and Yonetani, T. (1982) *J. Biol. Chem. 257*, 8766−8770.
58. Stein, P., Terner, J., and Spiro, T. G. (1982) *J. Phys. Chem. 86*, 168−170.
59. Scott, T. W., Friedman, J. M., Ikeda-Saito, M., and Yonetani, T. (1983) *FEBS Lett. 158*, 68−72.
60. Kaminaka, S., Ogura, T., Kitagishi, K., Tonetani, T., and Kitagawa, T. (1989) *J. Am. Chem. Soc. 111*, 3787−3794.
61. Hofrichter, J., Henry, E. R., Sommer, J. H., Deutsch, R., Ikeda-Saito, M., Yonetani, T., and Eaton, W. A. (1985) *Biochemistry 24*, 2667−2679.
62. Nagai, M., Kaminaka, S., Ohba, Y., Nagai, Y., Mizutani, Y., and Kitagawa, T. (1995) *J. Biol. Chem. 270*, 1636−1642.
63. Hirsch, R. E., Lin, M. J., Vidugirus, G. V. A., Huang, S., Friedman, J. M., and Nagel, R. L. (1996) *J. Biol. Chem. 271*, 372−375.
64. Wang, D., and Spiro, T. G. (1998) *Biochemistry 37*, 9940−9951.
65. Kavanaugh, J. S., Weydert, J. A., Rogers, P. H., and Arnone, A. (1998) *Biochemistry 37*, 4358−4373.
66. Hu, X., Dick, L. A., and Spiro, T. G. (1998) *Biochemistry 37*, 9445−9448.
67. Chi, Z., and Asher, S. A. (1998) *Biochemistry 37*, 2865−2872.
68. Kwiatkowski, L. D., Hui, H. L., Wierzba, A., Noble, R. W., Walder, R. Y., Peterson, E., Sligar, S., and Sanders, K. (1998) Preparation and Kinetic Characterization of a Series of βW37 Variants of Human HbA, Evidence for High Affinity T Quaternary Structures. *Biochemistry 37*, 4325−4335.
69. Shaanan, B. (1983) *J. Mol. Biol. 171*, 31−59.
70. Ishimuri, K., Hashimoto, M., Imai, K., Fushitani, K., Miyazaki, G., Morimoto, H., Wada, Y., and Morishima, I. (1994) *Biochemistry 33*, 2546−2553.
71. Togi, A., Ishimori, K., Unno, M., Konno, T., Morishima, I., Miyazaki, G., and Imai, K. (1993) *Biochemistry 32*, 10165−10169.

BI982724H